International Journal of Pharmaceutics 395 (2010) 215–221

Contents lists available at ScienceDirect

International Journal of Pharmaceutics

journal homepage: www.elsevier.com/locate/ijpharm

Online monitoring of particle mass flow rate in bottom spray fluid bed coating—Development and application

Li Kun Wang, Paul Wan Sia Heng, Celine Valeria Liew*

GEA-NUS Pharmaceutical Processing Research Laboratory, Department of Pharmacy, 18 Science Drive 4, National University of Singapore, Singapore 117543, Singapore

ARTICLE INFO

Article history:
Received 23 April 2010
Received in revised form 17 May 2010
Accepted 27 May 2010
Available online 4 June 2010

Keywords:
Coating
Pellets
Process analytical technologies (PAT)
Quality by design (QbD)
Particle mass flow rate

ABSTRACT

The primary purpose of this study is to develop a visiometric process analyzer for online monitoring of particle mass flow rate in the bottom spray fluid bed coating process. The secondary purpose is to investigate the influences of partition gap and air accelerator insert size on particle mass flow rate using the developed visiometric process analyzer. Particle movement in the region between the product chamber and partition column was captured using a high speed camera. Mean particle velocity and number of particles in the images were determined by particle image velocimetry and morphological image processing method respectively. Mass flow rate was calculated using particle velocity, number of particles in the images, particle density and size information. Particle velocity and number findings were validated using image tracking and manual particle counting techniques respectively. Validation experiments showed that the proposed method was accurate. Partition gap was found to influence particle mass flow rate by limiting the rate of solids flux into the partition column; the air accelerator insert was found to influence particle mass flow rate by a Venturi effect. Partition gap and air accelerator insert diameter needed to be adjusted accordingly in relation to the other variability sources and diameter of coating cores respectively. The potential, challenges and possible solutions of the proposed visiometric process analyzer were further discussed.

1. Introduction

Coating of multi-particulates is an important method for preparing modified release dosage forms (Cole, 1995; Porter, 2007). Bottom spray fluid bed coating is the main process for coating multi-particulates due to its ability to coat fine particles (Jones, 1994). For scaling up, one or more partition columns may be added into the product chamber of the bottom spray fluid bed coater, and the air distribution plates designed with highly perforated areas under the partition column(s). The highly perforated areas facilitate higher air velocity within the partition column, conveying particles upwards after they pass through the spray zone (Wurster, 1989; Christensen and Bertelsen, 1997; Wurster and Lincllof, 1966). The air velocity falls below the terminal velocity of the particles above the partition column due to the expansion of air in the broadening cross-sectional product chamber, causing particles to decelerate and fall outwards and back onto the staging annular bed surface (Christensen and Bertelsen, 1997; Wurster, 1989). Due to horizontal pneumatic transport aided by fluidization, particles were transferred through the partition gap again for the next coating cycle. Modifications had been made to the conventional Wurster coater by incorporating a swirl air accelerator—air accelerator insert accessory and enhanced coating performance was observed (Walter, 1998; Heng et al., 2006).

Under the quality by design (QbD) framework, coat uniformity is considered as a critical quality attribute for the particle coating process and hence variability sources affecting coat uniformity need to be identified and controlled (Nasr, 2006; Yu, 2008) (Fig. 1A). Bottom spray fluid bed coating is essentially a layering process and coat uniformity is largely affected by particle cycle-time distribution, which is defined as the time distribution for one particle's two consecutive passes through the spray zone (Cheng and Turton, 1994; Crites and Turton, 2005; Sudsakorn and Turton, 2000). Given a fixed load, particle mass flow rate (MFR) is inversely proportional to mean particle cycle-time, thus affecting coat uniformity. Hence, particle MFR is a source of variability in the bottom spray fluid bed coating process and needs to be monitored and controlled (Fig. 1B). Moreover, as "fountain-like" particle movement within the coater is the most basic characteristic flow pattern of the bottom spray fluid bed coating process, particle MFR measurement can serve to effectively monitor the continuous "fountain-like" particulate flow. For example, sudden reduction of MFR always indicates severe agglomeration while a sudden increase in MFR may be caused by deviation in air flow rate or atomizing air pressure. An unsteady particle mass flow rate suggests conditions of "choking" occurring within the partition column and air flow rate needs to be increased (Geldart and

* Corresponding author. Tel.: +65 65163870; fax: +65 67752265.
E-mail addresses: celineliew@nus.edu.sg, phalcv@nus.edu.sg (C.V. Liew).

0378-5173/$ – see front matter © 2010 Elsevier B.V. All rights reserved.
doi:10.1016/j.ijpharm.2010.05.044

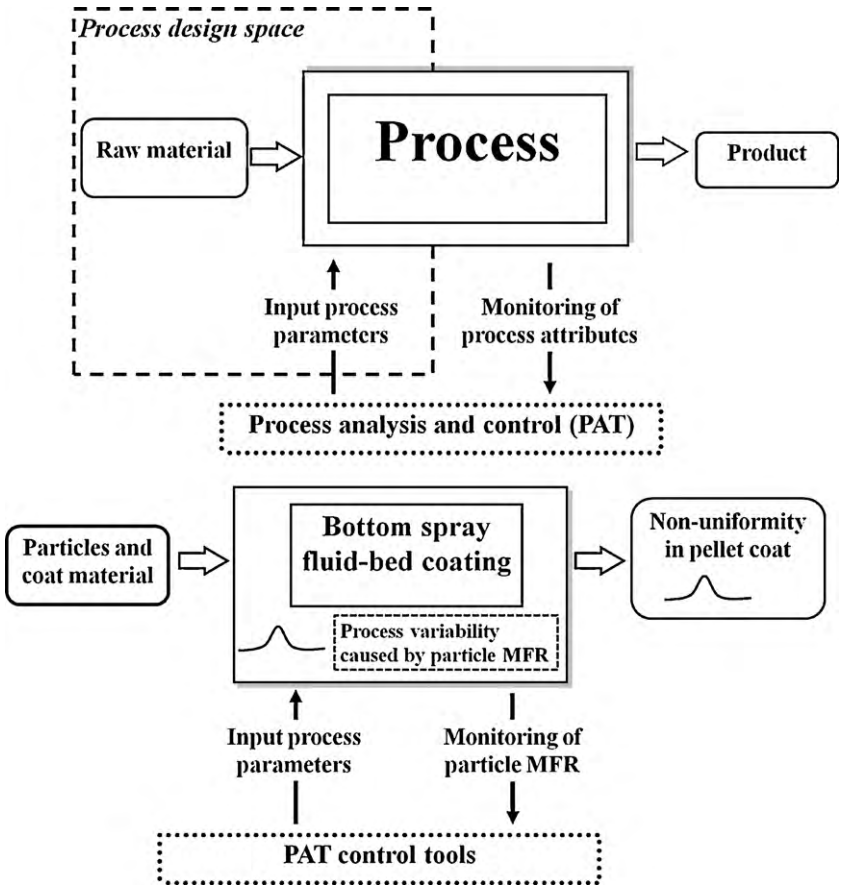

Fig. 1. (A) Role of PAT under QbD framework (adapted from Nasr, 2006) and (B) the need for monitoring of particle MFR in bottom spray fluid bed coating.

Rhodes, 1985; Bi et al., 1993; Grace and Bi, 1996). Hence, it is highly desirable to develop a process analyzer for quantifying particle MFR in bottom spray fluid bed coating.

The current MFR measurement method collects particles by placing an additional particle collector inside the product chamber, stopping particle cycling and recording the time taken for all the particles to flow into the collector (Chan et al., 2006). MFR can be calculated according to the following equation:

$$\text{MFR} = \frac{M_t}{t} \tag{1}$$

where M_t is the load of particles and t is the time taken for all the loaded particles to flow into the collector (Chan et al., 2006). Nevertheless, there are several limitations associated with this method of measurement. Firstly, MFR can only be measured at the start of the process, when the fluidizing air and MFR have yet to stabilize. Secondly, this method cannot be extended for online measurement as particles were stopped from undergoing further coating cycles. As such, it is highly desirable to develop a new method that is able to accurately measure particle MFR online for bottom spray fluid bed coaters.

Particle MFR through a measured volume can also be determined using another principle:

$$\text{MFR} = \frac{M_V \times \bar{v}}{L} \tag{2}$$

where M_V is the total mass of particles within the measured volume; $\bar{v}$ is the mean particle velocity within the measured volume; L is the length of the measured volume along the direction of particle movement. As multi-particulates are usually uniform in size and shape, M_V can be calculated using the following equation:

$$M_V = N_p \times \rho \times V_p \tag{3}$$

where ρ and V_p are the density and volume of a single particle respectively and N_p is the number of particles in the measured volume. Hence, particle MFR can be determined as long as the mean velocity and number of particles within the measurement volume can be estimated.

In this study, the downward particle movement between partition column and product chamber was captured using a high speed camera. The mean particle velocity was determined using particle image velocimetry (PIV) method; mass of particles within the measurement volume was estimated using particle size, density and particle number information obtained from morphological image processing. The proposed process analyzer, a visiometric process analyzer according to the definition given by Liew et al. (2010), would also be employed to illustrate the roles of partition gap and air accelerator insert (AAI) as their roles in bottom spray fluid bed coating could be better understood.

2. Materials and methods

2.1. Materials

Nonpareils (710–850 μm size fraction, 1.72 g/cm^3 particle density, Hanns G. Werner's, Tornesh, Germany) were base-coated to 10% (w/w) using hydroxypropyl methylcellulose (Methocel E-3 LV, The Dow Chemical Company, Midland, MI, USA) to protect particle integrity. The particles were used as seed particles for visualizing downward particle movement in the bottom spray fluid bed coater.

2.2. High speed imaging

A load of 1 kg base-coated nonpareils was introduced into the product chamber of a bottom spray fluid bed coater (Precision Coater, MP-1, GEA Aeromatic-Fielder, Eastleigh, Hampshire, UK). A transparent acrylic product chamber was used to facilitate high speed imaging (Fig. 2A). The downward particle movement within a 1.5 cm by 1.5 cm area between product chamber and partition column was captured using a high speed video camera (MotionPro HS-3, Redlake, Tallahassee, FL, USA) (Fig. 2B). Various combinations of process conditions were employed (Table 1). The schematic diagram of AAI is shown in Fig. 2C. The high speed camera was programmed and controlled using Matlab (R2007b, The Mathworks, Natick, MA, USA) such that the camera took 50 video clips in a 2 Hz pulsed mode for each combination of process conditions. Each video clip consists of 50 frames of images, which were taken at a recording speed of 4000 frames/s. The image size was 248 pixels by 248 pixels.

2.3. Particle image velocimetry (PIV)

High speed images were interrogated using PIV to determine particle velocity information (Fig. 3A). In PIV, the first sequential frame was divided into sub images for roaming in the second frame. The displacement of a sub image was determined by searching the maximum image similarity between the roaming sub image and corresponding sub image in the second frame (Adrian, 1988, 1991; Adrian and Yao, 1985; Keane and Adrian, 1992; Westerweel, 1993, 1997). Cross-correlation and minimum quadratic difference (MQD) are two available methods for quantification of image similarities (Suh, 2003). In this study, MQD method was selected due to its robustness. In the MQD method, the quadratic difference C (ΔX, ΔY) between two sub images, f_1 and f_2, is expressed as:

$$C(\Delta X, \Delta Y) = \sum_{i=1}^{N}\sum_{j=1}^{N} |f_1(X_i, Y_j) - f_2(X_i + \Delta X, Y_j + \Delta Y)| \quad (4)$$

where X_i, Y_j are the coordinates; ΔX, ΔY are the displacements along the coordinates; f_1 and f_2 are the first and second images respectively (Suh, 2003). The detection window size was set as 64 pixels by 64 pixels and the overlapping ratio was set as 50%.

2.4. Morphological image processing

Morphological image processing extracts relevant structures of the image by probing the image with another set of known shape called structuring element (Soille, 2003a). The flow chart of basic morphological image processing is shown in Fig. 3B, and image processing was performed using Matlab.

Morphological image processing usually employs a combination of elementary operations such as dilation and erosion. The grey-scale dilation and erosion of image f are defined as:

$$(f \oplus b)(x, y) = \max\{f(x - x', y - y') + b(x', y') \in D_b\} \quad (5)$$

and

$$(f \Theta b)(x, y) = \min\{f(x + x', y + y') - b(x', y') \in D_b\} \quad (6)$$

respectively, where b is the structuring element and D_b is the domain of b (Gonzalez et al., 2004).

The grey-scale opening $f \circ b$ of an image f is defined (Gonzalez et al., 2004) as:

$$f \circ b = (f \Theta b) \oplus b \quad (7)$$

A flat and disk shape structuring element of 2-pixel diameter was used in the opening operation. Grey-scale opening suppressed bright details that were smaller than the structuring element.

Regional maxima are connected components of pixels with a constant intensity value with all the external boundary values having smaller intensity values. In this study, the regional maxima were set as 1 and all the other pixels were set as 0 (Soille, 2003b). Regional maxima operation after grey-scale opening marked individual particles as white dots on the binary images.

Image reconstruction dilates a marker image with respect to the mask image until stability is achieved (Soille, 2003b). Image labelling sets all the pixels belonging to a connected component of the input binary image to a specific grey-scale level value. Different grey-scale values are used for each of the connected components and the assigned grey-scale values are referred as labels. The number of labels corresponded to the number of connected components and hence the number of particles in the image that are counted (Soille, 2003a). Within the context of the following sections, particle number refers to the total number of particles on a given image.

2.5. Calculation of particle MFR using particle velocity and particle number information

The particle MFR was calculated using the following equation:

$$\mathrm{MFR} = \frac{\bar{v} \times n \times V_p \times \rho}{L} \times \frac{S_t}{S_m} \quad (8)$$

where $\bar{v}$ is the average velocity obtained from PIV results; n is the particle number in each image, which was obtained using morphological image processing; V_p is the mean volume of a single particle; ρ is the particle density; L is the height of the captured area along the vertical direction, and S_t and S_m are the total and measured cross-sectional areas respectively (Fig. 2B).

2.6. Validation of PIV and morphological image processing results

The particles from 20 video clips were tracked for validation of particle velocity using a third party image tracking software (TEMA 2.6, Image Systems AB, Linkoping, Sweden). All the particles in the first frame and the 25th frame were tracked through the 50-frame video clips. In addition, 20 randomly chosen frames were counted manually to cross-validate the morphological image processing results. The average particle MFR was calculated using Eq. (8).

3. Results

3.1. PIV and morphological image processing results

A sample of the PIV results is shown in Fig. 3A(ii). The velocity vectors were successfully detected using MQD-PIV method. Most velocity vectors were detected to point downwards within a narrow velocity magnitude range.

Fig. 3B shows samples of processed images for the various morphological image processing steps. After grey-scale opening, intensity changes that were smaller than 2 pixels were suppressed (Fig. 3B(ii)). Particles on the image were then detected using local maxima operation (Fig. 3B(iv)). However, the local maxima located outside the particles were also detected. Any false positive particle detection was removed by intersecting the local maxima image with the border-cleared image (Fig. 3B(iv) and (v)). The intersection was then reconstructed to link the broken parts from the same particles using a thresholding operation (Fig. 3B(vii)). The number of labels corresponded to the number of particles on the image after the labelling operation (Fig. 3B(viii)).

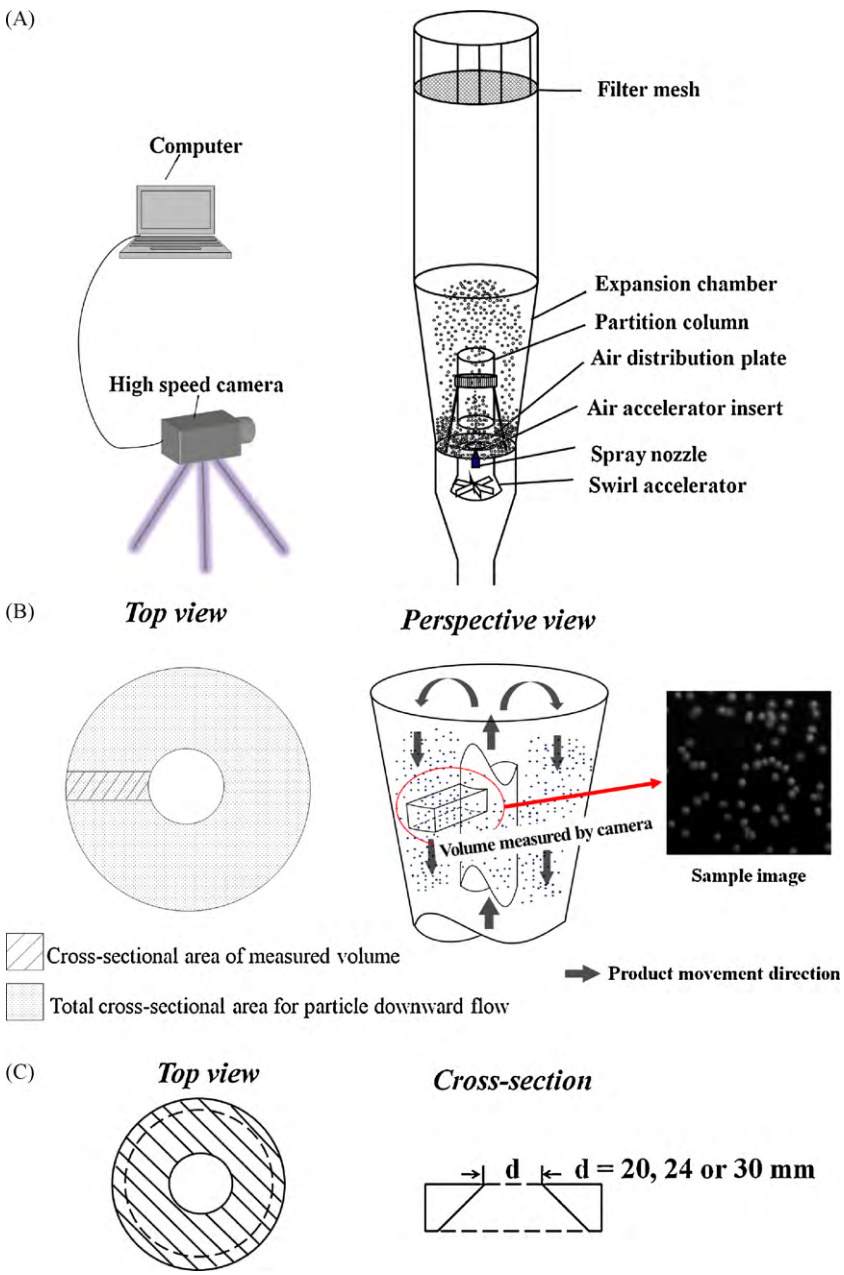

Fig. 2. Schematic diagram of (A) high speed imaging, (B) measured volume with respect to product chamber and (C) AAI with diameter of *d*.

3.2. Validation results of PIV and morphological image processing

The mean vertical displacement components detected by PIV from 20 video clips were plotted against mean particle displacement obtained from the particle tracking method (Fig. 4A). It was observed that particle displacement obtained from the PIV method was similar to that of the validation data (root mean squared error (RMSE) = 0.1893 pixels). The validation results of the proposed morphological image processing method are shown in Fig. 4B (RMSE = 1.8974). The RMSEs for both PIV and morphological image processing results were less than 3% of the mean values, showing good accuracy and robustness of the proposed method.

3.3. Influences of partition gap and AAI diameter on MFR

The effects of partition gap and air flow rate on particle MFRs were plotted and shown in Fig. 5A. It was observed that the particle MFR generally increased with partition gap and air flow rate

Table 1
Process parameters for MFR measurement.

Measurement	Air flow rate (m^3/h)	Atomizing air pressure (bar)	Partition gap (mm)	AAI diameter (mm)
A*	80, 90, 100, 110, 120	2.0	5, 10, 15, 20, 25	24
B*	90	1.0, 1.5, 2.0, 2.5, 3.0	10	20, 24, 30, 40

A* process parameters for mapping the influence of air flow rate and partition gap on particle MFR.
B* process parameters for mapping the influence of atomizing air pressure and AAI diameter on particle MFR.

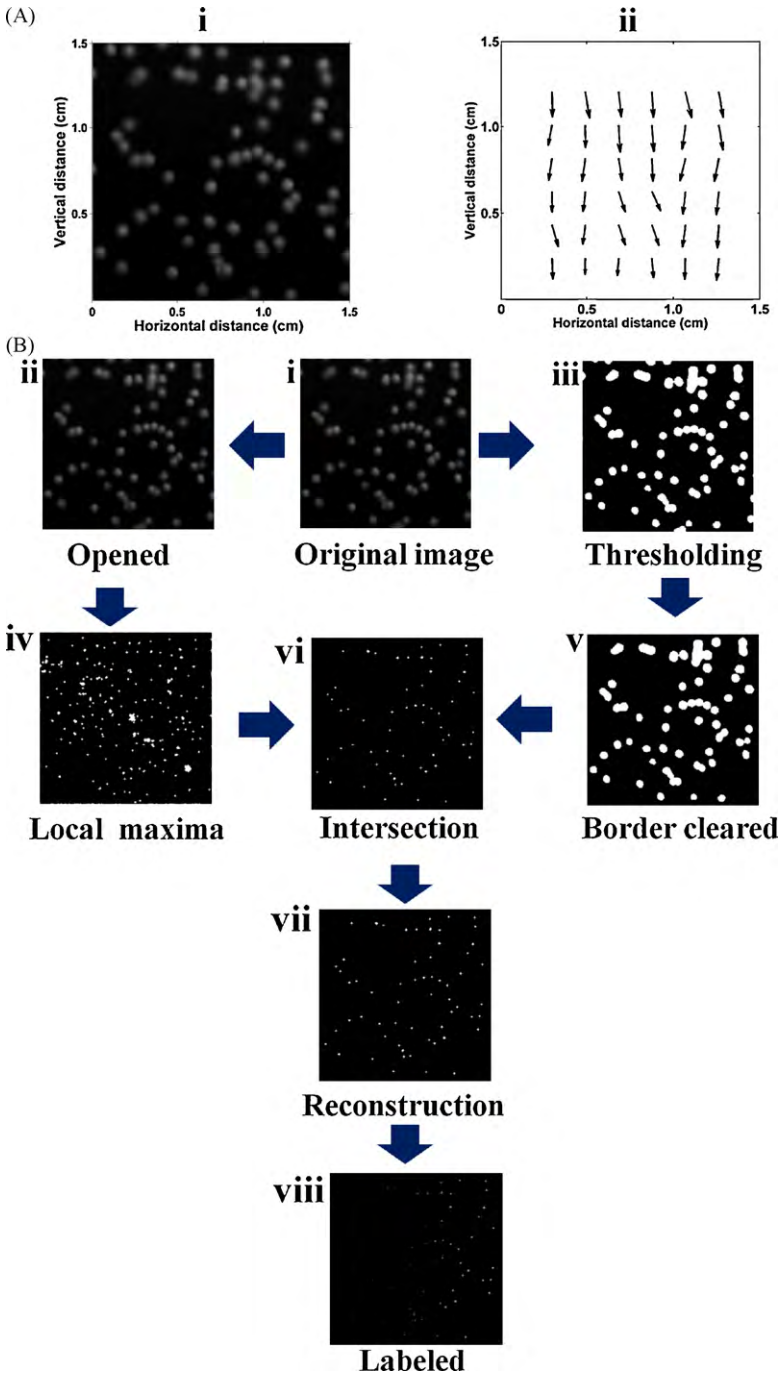

Fig. 3. (A) Sample high speed images and PIV result and (B) sample processed images from each step of morphological image processing flow chart.

before levelling off at a higher air flow rate. It was also observed that particle MFR increased with higher atomizing air pressure, but decreased when an AAI with larger diameter was used (Fig. 5B). The trends are in accordance with findings from a previous study (Chan et al., 2006).

4. Discussion

4.1. Comparative advantageous of measuring downward moving particles

Measuring upward moving particles within the partition column is an alternative technique to determine particle MFR. However, it is important to point out that measuring MFR within the partition column is not preferred due to a few reasons. Firstly, voidage within the partition column is much lower than that in the region between product chamber and partition column. All the particles within the partition column cannot be fully captured by the camera due to shielding by particles in the near wall region within the partition column. This may cause inaccurate particle velocity estimations as only a limited fraction of particles appeared on each image. Erroneous particle counting could also occur due to this reason. Secondly, the velocities of upward moving particles in the partition column are much higher than those of falling particles at the periphery. Video capture must be operated at much higher speeds to freeze particle movement. In this case, timely data processing becomes computationally complicated and costly. Thirdly,

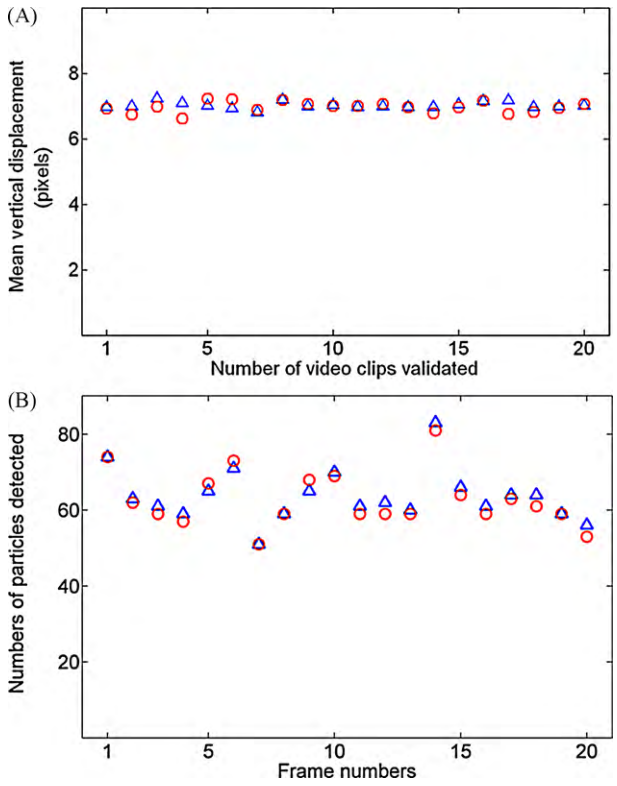

Fig. 4. (A) Validation (○) and PIV results (Δ) of particle displacements and (B) validation (○) and morphological image processing results (Δ) for the number of particles appeared on the image.

the particle velocities within the partition column vary from downward moving particles joining recirculation to high speed upward moving particles at the center of the partition column (Palmer et al., 2006; Bi and Pugsley, 2007). This results in less accurate estimation of mean particle velocity. Lastly, not only is the interior of the partition column not easily captured, the coating process also makes it considerably "dirtier" with many adhering spray droplets and fines due to attrition. Hence, less fouling conditions exist if images were captured from a view between the product chamber and partition column.

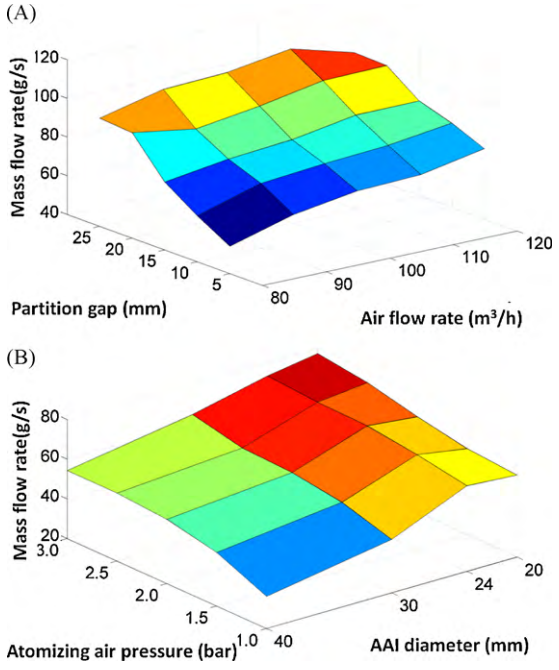

Fig. 5. (A) Influences of partition gap and air flow rate on particle MFR and (B) influence of atomizing air pressure and AAI diameter on particle MFR.

4.2. The role of partition gap

It has been shown that particle MFR generally increases with higher partition gap. This is because the height of the partition gap limited the rate of solids flux into the partition column. The levelling off trend may be attributed to intense turbulent air flow under high solids content conditions, which caused cluster formation and sedimentation/recirculation of particulates, thus limiting the particle MFR from increasing. Clustering and sedimentation under high solids content and turbulent air flow conditions are well known phenomena in circulating fluid bed systems (Horio, 1997). Similar flattening trend was also reported using the Wurster coater (Chan et al., 2006). According to the bottom spray fluid bed coating models developed in several papers (Cheng and Turton, 1994; Crites and Turton, 2005; Sudsakorn and Turton, 2000), a higher MFR usually results in a shorter mean particle cycle-time. This allows particles to undergo more coating cycles per unit time provided that the other conditions are kept constant, thus a more uniform coat layer can be expected.

4.3. AAI diameter and the effectiveness of Venturi effect

It was reported that the main mechanism of particle feeding in the Precision Coater is by the Venturi effect (Chan et al., 2006). Venturi effect occurs when fluid passes through a smooth and narrow orifice with a fixed fluid flow rate (Nakayama and Boucher, 1999). Due to the fixed fluid flow rate and smaller cross-sectional area near the AAI orifice, the fluid velocity increased to maintain air flow rate. According to the law of energy conservation, the fluid pressure dropped above the AAI orifice, bringing about a suction pressure at the bottom of the partition column. As demonstrated above, particle MFR increased with higher air flow rate, higher atomizing air pressure and smaller AAI size. This was because higher air flow rate and atomizing air pressure caused higher air velocity through the AAI orifice, inducing a lower pressure above the AAI orifice. Similarly, AAIs with smaller diameters caused higher air velocities at the orifice, hence inducing lower pressures at the base of the partition column, drawing more particles into the partition column. Hence, for coating of multi-particulates, AAIs with smaller diameters might be advantageous by contributing higher MFR. However, this trend may not hold for powder coating due to two reasons. Firstly, compared with free-flowing multi-particulates, powders are usually more cohesive and have relatively poor flowability. Thus, it might be difficult for the powder to flow easily into the partition column even with the help of a stronger Venturi effect. Hence, promoting powder flow by adopting larger diameter AAIs may be more effective than just relying on the Venturi effect alone. Secondly, arch formation is a well know phenomenon where powders flow through an orifice due to frictional force and particle elasticity (Duran, 1998, 2000; Cooper, 2001). Hence, AAIs with smaller diameters are more likely to promote arch formation as powders are exposed to frictional forces over a longer distance before being conveyed. As such, a combination of AAI with a larger diameter and larger partition gap is suggested for powder coating or bottom-spray granulation processes.

4.4. Uses and integration of online MFR measurement

As demonstrated, the proposed method for measuring particle MFR was accurate, non-invasive and useful for enumerating bottom spray fluid bed coating. With only a small transparent area (a 1.5 cm

by 1.5 cm square in this study) on the product chamber needed for measuring particle MFR, a process monitoring camera can be easily integrated on an observation window in the bottom spray fluid bed coater for online MFR monitoring. Moreover, a relatively small image size ensures fast PIV and morphological image processing. As an example, it took less than 5 s to complete a MFR measurement using a desktop PC. Moreover, it is worthwhile to point out that the proposed method may need modification for use in large scale coaters. This is mainly because the distance between the product chamber and partition column is much longer and a lens with sufficient depth of field is required. In this situation, modifications to the proposed process analyzer may be needed to provide adequate illumination. Moreover, corrections for images distorted by lens distortion may also be used. Volume illumination using a laser light source with optics may be employed to provide an intense and spatially confined light beam. Camera calibration techniques can be used for large scale coating process monitoring to ensure measurement accuracy.

Real-time MFR measurements can also be used to control spray rate and prevent agglomeration in the spray zone. It is generally agreed that agglomeration arises when the particles are overwetted and liquid bridges form between particles. Under a fixed spray rate, with a higher MFR, the atomized coating fluid deposits on more particles and over-wetting conditions are less likely to rise. Hence, particle-fluid flow ratio (PFFR) was proposed to quantify the balance status between particle MFR and coating fluid spray rate. PFFR is defined as:

$$\mathrm{PFFR} = \frac{\mathrm{MFR}}{\mathrm{SR}} \tag{9}$$

where MFR is the particle mass flow rate and SR is the spray rate of the coating fluid. A minimum PFFR can be measured experimentally and the coating process may be controlled directly based on PFFR in order to facilitate coating speed. During coating process scale-up, process parameters can be tuned to keep the same PFFR as the pilot scale coater to avoid agglomeration.

5. Conclusions

A mass flow measurement method based on PIV and morphological image processing was developed. Validation showed that the proposed method was both accurate and robust experimentally. The role of partition gap was found to limit the maximum solids flux rate under a certain air flow rate. AAIs with smaller diameters were suggested for multi-particulate coating and AAIs with larger diameters were better for small particle coating or granulation. Besides revealing the potential of online MFR measurement, the integration of proposed process analyzer with bottom spray fluid bed coater was also discussed. For large scale coaters, intense laser lighting and careful camera calibration were suggested for successful implementations.

References

Adrian, R., 1988. Double exposure, multiple-field particle image velocimetry for turbulent probability density. Opt. Laser Eng. 9, 211–228.

Adrian, R., Yao, C., 1985. Pulsed laser technique application to liquid and gaseous flows and the scattering power of seed materials. Appl. Optics 24, 44–52.

Adrian, R.J., 1991. Particle-imaging techniques for experimental fluid mechanics. Annu. Rev. Fluid Mech. 23, 261–304.

Bi, H.T., Grace, J.R., Zhu, J.X., 1993. On types of choking in pneumatic systems. Int. J. Multiphase Flow 19, 1077–1092.

Bi, X., Pugsley, T., 2007. Investigation of the sources of variability in the Wurster coater: analysis of particle cycle times using PEPT. In: Berruti, F. (Ed.), 2007 ECI Conference on The 12th International Conference on Fluidization—New Horizons in Fluidization Engineering. The Berkeley Electronic Press, Vancouver, pp. 431–440.

Chan, L.W., Tang, E.S.K., Heng, P.W.S., 2006. Comparative study of the fluid dynamics of bottom spray fluid bed coaters. AAPS PharmSciTech 7, 37–46.

Cheng, X.X., Turton, R., 1994. The uniformity of particle coating occurring in fluidized beds. In: Weimer, A.W., Chen, J.C., Fan, L.-S., Yang, W.-C. (Eds.), Fluid Particle Technology: Analysis and Applications. American Institute of Chemical Engineers, New York, pp. 145–152.

Christensen, F.N., Bertelsen, P., 1997. Qualitative description of the Wurster-based fluid-bed coating process. Drug Dev. Ind. Pharm. 23, 451–463.

Cole, G., 1995. Introduction and overview of pharmaceutical coating. In: Cole, G. (Ed.), Pharmaceutical Coating Technology. Taylor & Francis, Bristol, pp. 1–5.

Cooper, P., 2001. Practical solutions to critical solids handling problems. In: Hoyle, W. (Ed.), Powders and Solids: Developments in Handling and Processing Technologies. UK, Royal Society of Chemistry, Cambridge, pp. 29–41.

Crites, T., Turton, R., 2005. Mathematical model for the prediction of cycle-time distributions for the Wurster column-coating process. Ind. Chem. Eng. Res. 44, 5397–5402.

Duran, J., 1998. Static and dynamic arching effect in granular materials. In: Hermann, H.J., Hovi, J.-P., Luding, S. (Eds.), Physics of Dry Granular Media. Kluwer Academic Publishers, Boston, pp. 197–216.

Duran, J., 2000. Sands, Powders, and Grains. Springer, New York, pp. 9–12.

Geldart, D., Rhodes, M.J., 1985. From minimum fluidization to pneumatic transport—a critical review of the hydrodynamics. In: Basu, P. (Ed.), Circulating Fluidized Bed Technology: Proceedings of the First International Conference on Circulating Fluidized Beds. Pergamon Press, Nova Scotia, pp. 21–31.

Gonzalez, R.C., Woods, R.E., Eddins, S.L., 2004. Morphological image processing. In: Gonzalez, R.C., Woods, R.E., Eddins, S.L. (Eds.), Digital Image Processing using MATLAB. Pearson Prentice Hall, Upper Saddle River, pp. 335–377.

Grace, J.R., Bi, H., 1996. Introduction to circulating fluidized beds. In: Grace, J.R., Avidan, A.A., Knowlton, T.M. (Eds.), Circulating Fluidized Beds. Blackie Academic & Professional, London, pp. 10–14.

Heng, P.W.S., Chan, L.W., Tang, E.S.K., 2006. Use of swirling airflow to enhance coating performance of bottom spray fluid bed coaters. Int. J. Pharm. 327, 26–35.

Horio, M., 1997. Hydrodynamics. In: Grace, J.R., Avidan, A.A., Knowlton, T.M. (Eds.), Circulating Fluidized Beds. Blackie Academic & Professional, London, pp. 21–42.

Jones, D., 1994. Air suspension coating for multiparticulates. Drug Dev. Ind. Pharm. 20, 3175–3206.

Keane, R.D., Adrian, R.J., 1992. Theory of cross-correlation analysis of PIV images. Appl. Sci. Res. 49, 191–216.

Liew, C.V., Wang, L.K., Heng, P.W.S., 2010. Development of a visiometric process analyzer for real-time monitoring of bottom spray fluid-bed coating. J. Pharm. Sci. 99, 345–356.

Nakayama, Y., Boucher, R.F., 1999. Introduction to Fluid Mechanics. John Wiley & Sons Inc., New York, pp. 42–45.

Nasr, M., 2006. FDA's quality initiatives: an update. http://www.gmp-compliance.com/daten/download/FDAs_Quality_Initiative.pdf (accessed August 2009).

Palmer, S.E., Seville, J.P.K., Ingram, A., Fitzpatrick, S., Fan, X., 2006. Tracking pellet motion in a Wurster coater using positron emission. In: Fifth World Congress on Particle Technology (Session #158b) on 2006 AIChE Spring National Meeting, Orlando, American Institute of Chemical Engineers.

Porter, S.C., 2007. Coating of tablets and multiparticulates. In: Aulton, M.E. (Ed.), Aulton's Pharmaceutics—The Design and Manufacture of Medicines. Churchill Livingstone, New York, pp. 500–514.

Soille, P., 2003a. Morphological Image Analysis: Principles and Applications, 2nd ed. Springer, New York, pp. 1–12.

Soille, P., 2003b. Morphological Image Analysis: Principles and Applications, 2nd ed. Springer, New York, pp. 219–238.

Sudsakorn, K., Turton, R., 2000. Nonuniformity of particle coating on a size distribution of particles in a fluidized bed coater. Powder Technol. 110, 37–43.

Suh, Y.K., 2003. Multi-frame MQD-PIV. KSME Int. J. 17, 1552–1562.

Walter, K., 1998. Apparatus for coating solid particles. US Patent No. 5,718,764.

Westerweel, J., 1993. Digital particle image velocimetry: theory and application. Ph.D. Thesis, Technische Universiteit Delft, The Netherlands.

Westerweel, J., 1997. Fundamentals of digital particle image velocimetry. Meas. Sci. Technol. 8, 1379–1392.

Wurster, D.E., 1989. Particle-coating methods. In: Lieberman, H.A., Lachman, L., Schwartz, J.B. (Eds.), Pharmaceutical Dosage Forms: Tablets. Dekker, New York, pp. 161–195.

Wurster, D.E., Lincllof, J.A., 1966. Particle Coating Apparatus. US Patent No. 3,241,520.

Yu, L.X., 2008. Pharmaceutical quality by design: product and process development, understanding, and control. Pharm. Res. 25, 781–792.